Electronic structure of trigonal and amorphous Se and Te†

J. D. Joannopoulos,* M. Schlüter,‡ and Marvin L. Cohen
Department of Physics, University of California, Berkeley, California 94720
and Inorganic Materials Research Division, Lawrence Berkeley Laboratory, Berkeley, California 94720
(Received 25 July 1974)

The electronic structure of trigonal and amorphous Se and Te is investigated using the empirical pseudopotential method (EPM), charge-density calculations, and simple tight-binding models. Band structures and electronic densities of states are obtained which are in excellent agreement with recent photoemission measurements. The tight-binding models are used to obtain analytic expressions for the energy bands and to interpret the EPM band structures in terms of real-space orbital-orbital interactions. Charge-density calculations obtained as a function of energy and evaluated within specific energy intervals are used to interpret various structure in the density of states. Specifically certain easily resolvable peaks in the experimental photoemission spectra are associated with intrachain and interchain localized states, respectively. By taking only short-wavelength components of the charge density, a bonding charge can be defined which gives an estimate of the intrachain vs interchain bonding strengths. The trigonal results along with model calculations to investigate the effects of bond-angle variations on chains and the presence of eight- and six-fold rings of bonds are used to interpret the changes observed in the experimental spectra of amorphous Se and Te. A new model of amorphous Se is proposed.

I. INTRODUCTION

To gain a good understanding of the electronic structure of any system it is important to study the electronic density of states of this system. The main reasons for this are that the density of states contains information which is easily accessible and (i) remains a well-defined quantity regardless of structure, (ii) is sensitive to effects of periodicity, (iii) contains basic information about the bonding nature of the system, (iv) is sensitive to the topology of the system, and (v) reflects the intrinsic atomic nature of the systems constituents.

A thorough study of the electronic density of states should involve a realistic calculation to facilitate comparisons with experiment, a careful examination of the calculated spectra (e.g., in terms of charge distributions), and simple model calculations that can aid in interpreting main features in a simple physical way. Experimentally, information about the density of states can be obtained from ultraviolet (UPS) and x-ray (XPS) photoemission measurements as well as x-ray emission and absorption experiments. The trigonal and amorphous phases of Se and Te are excellent systems for the study described above since new UPS[1] and XPS[1-3] measurements have provided important information about all the valence bands and have revealed many inadequacies of current theoretical calculations.[4-7] In one of these calculations[4] a complete merging of the s- and p-like bands was proposed; this disagrees qualitatively with the recent photoemission data. Other calculations[5-7] show a separation of s- and p-like bands which is in qualitative agreement with photoemission experiments, however, bandwidths and important structure are not correct. In addition, no calculations exist giving a detailed analysis of the electronic nature of structure in the density of states. The photoemission measurements also show some remarkable differences between the trigonal and amorphous phases.

We thus present in this paper new calculations of the band structure, densities of states, and charge densities for trigonal Se and Te using the empirical pseudopotential method (EPM).[8] We also introduce simple tight-binding models described by a set of parameters which are related to important physical interactions in the system. In addition, we have calculated the densities of states for various model structures as an aid in interpreting the amorphous photoemission results.

The format of the paper is as follows. In Sec. II we discuss the structural aspects of Se and Te. In Sec. III we discuss the method and parameters used in our EPM calculations, and we introduce and discuss two tight-binding models. In Sec. IV we present the results of our calculations for trigonal Se and Te using the EPM and tight-binding models, and we give a new interpretation of the photoemission spectra. In Sec. V we present our model calculations, and we discuss and interpret the amorphous spectra. Finally, in Sec. VI we make some concluding remarks.

II. STRUCTURAL CONSIDERATIONS

The crystal structure of trigonal Se and Te consists of helical chains which spiral around axes parallel to the crystalline c axis. The helices are

arranged in an hexagonal array. The crystal unit cell consists of three atoms of one helix and is shown in Fig. 1(a). The space groups of trigonal Se and Te are D_3^4 or D_3^6, depending on the sense of rotation of the helical chains. The existence of chains is manifested by the fact that each atom is tightly covalently bonded to two neighbors, as one would expect for elements with six valence electrons.[9] The bonding between individual chains is much weaker and is often believed to be of van der Waals character. We shall, however, show in this paper that there is definitely some covalentlike bonding between neighboring chains. The anisotropy ratio of *intra*chain bonding strength versus *inter*chain bonding strength decreases in going from Se to Te. This is reflected in their mechanical properties[10] and in the ratio of interchain versus intrachain atomic distances d_2/d_1 =1.49 for Se and 1.31 for Te. In fact the next-heavier group-VI element Po crystallizes in an isotropic simple cubic structure into which Te and Se transform under hydrostatic pressures of about 60 and 130 kbar, respectively.[10] The close relationship between the trigonal structures of Se and Te and the simple cubic structure can be recognized by comparing Figs. 1(a) and 1(b). A rough picture of the electronic structure of Se and Te can be obtained by considering the strong intrachain bonding only. Since the atomic s states are well separated from the higher p states (~10 eV for Se and ~8 eV for Te), it is expected that s-p mixing will be small in the crystal. This does not at all contradict a bond angle of about 104° if one allows for slight mixing with d states as well.

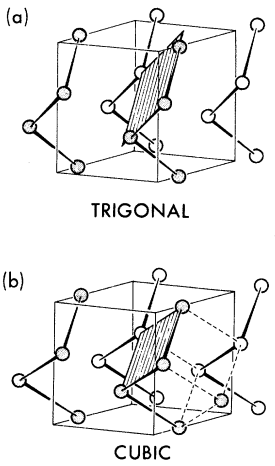

FIG. 1. (a) Unit cell of trigonal Se and Te. The plane in which charge densities are represented is indicated as a shaded area. (b) Corresponding simple cubic structure from which the structure of Se and Te can be derived by trigonal distortions.

In fact, we obtained from our pseudopotential calculations by angular projection about (5–10)% s and (1–5)% d admixture to the bonding p states. The deep-lying s states overlap on neighboring atoms and combine into bondinglike and antibondinglike states. Since there is only one s state per atom available, two complete covalent bonds per atom cannot be accomplished this way. As in a metal there will be *no* gap between these s states, and since all states are fully occupied the net contribution of the s states to the cohesive energy will be small. The two bonds per atom are thus essentially formed by p states with small admixtures of s and d character. This leaves one nonbonding p state per atom. The six electrons per atom therefore occupy the s states, the bonding p-like states, and the nonbonding or lone-pair states. The Fermi level falls between the nonbonding and the antibonding p-like states.

III. CALCULATIONAL METHODS

A. EPM and bonding charge model

The EPM has been previously discussed extensively.[8] The values of the atomic form factors used in our calculations were obtained by fitting peaks in the density of states to the structure in experimental photoemission spectra.[1,2] To obtain good convergence we used about 60 plane waves as a basis set with an additional 300 plane waves through a perturbation technique developed by Löwdin.[11] We calculated $E(\vec{k})$ in $\frac{1}{12}$ of the Brillouin zone at 300 grid points. The density of states was then obtained using

$$N(E) = \frac{1}{NN_a} \sum_n \sum_{\vec{k}} \delta(E - E_n(\vec{k})), \tag{1}$$

where N_a is the number of atoms in the primitive cell, N is the number of primitive cells, and $N(E)$ is normalized to the number of states per atom. The method of Gilat and Raubenheimer[12] is used to evaluate the integral in Eq. (1). The energy derivatives required by this method were obtained using $\vec{k}\cdot\vec{p}$ perturbation theory.

Once we have the energies $E_n(\vec{k})$ and the pseudowave functions $\phi_{n,\vec{k}}(\vec{r})$ for each band n, we can define[13] an average "energy" charge density $\rho_E(\vec{r})$ by

$$\rho_E(\vec{r}) = e \sum_n \sum_{\vec{k}} \delta(E_n(\vec{k}) - E) |\phi_{n,\vec{k}}(\vec{r})|^2. \tag{2}$$

This can then be used to define $\rho_{E_f,E_i}(\vec{r})$ for an interval $[E_i, E_f]$ by

$$\rho_{E_f,E_i}(\vec{r}) = \int_{E_i}^{E_f} \rho_E(\vec{r})\, dE. \tag{3}$$

ρ_{E_f,E_i} is a very useful quantity for studying the distribution and character of the electrons in various regions $[E_i, E_f]$ of the density of states. Since $\rho_{E_f,E_i}(\vec{r})$ is periodic, we can expand it as

$$\rho_{E_f,E_i}(\vec{r}) = \sum_{\vec{G}} \hat{\rho}_{E_f,E_i}(\vec{G}) e^{i\vec{G}\cdot\vec{r}}. \tag{4}$$

We can now go a step further and isolate the short-wavelength Fourier components from the long-wavelength Fourier components,

$$\rho_{E_f,E_i}(\vec{r}) = \rho^L_{E_f,E_i}(\vec{r}) + \rho^S_{E_f,E_i}(\vec{r}), \tag{5}$$

with

$$\rho^S_{E_f,E_i}(\vec{r}) \equiv \sum_{|\vec{G}| \geq 2\pi/\lambda_0} \hat{\rho}_{E_f,E_i}(\vec{G}) e^{i\vec{G}\cdot\vec{r}}, \tag{6a}$$

$$\rho^L_{E_f,E_i}(\vec{r}) \equiv \sum_{|\vec{G}| < 2\pi/\lambda_0} \hat{\rho}_{E_f,E_i}(\vec{G}) e^{i\vec{G}\cdot\vec{r}}. \tag{6b}$$

This introduces a new method of defining bonding charges and a way to separate out the effects of metallicity. The cutoff or boundary wavelength λ_0 between short- and long-wavelength components was found to lie naturally at $\lambda_0 = d$, where d is the nearest-neighbor separation in Se or Te.

B. Tight-binding model with only intrachain interactions

We now introduce a very simple tight-binding model in which we include only intrachain interactions. This model can be solved analytically, and it contains the basic information for understanding the EPM band structures and the importance of a single chain as a unit. This model is particularly applicable to Se, which is more anisotropic than Te. In the next section we will also include interchain interactions; so the extended model will be applicable to both Se and Te.

We begin by assigning to each atom a basis set consisting of an s-like orbital $|s\rangle$, two hybrid and mixed p-like orbitals $|p\rangle$, and one lone-pair $|l\rangle$ function. These orbitals are shown schematically in Fig. 2(a). The $|s\rangle$ orbitals constitute wave functions which are localized on the atoms and are essentially the atomic s-states of Se or Te. The $|p\rangle$ orbitals are primarily of atomic p nature, but also contain some s and d admixture. They are primarily concentrated along the bonds in the chain with small lobes at antibonding sites. Finally, the lone-pair $|l\rangle$ orbitals are taken to be pure atomic p functions. We can now write down a Hamiltonian for the chain which is essentially "one dimensional" and has the form

$$H = \sum_{i,i'} V_S^{i,i'} |s_i\rangle\langle s_{i'}|$$
$$+ \sum_{\substack{i,i' \\ j,j'}} V_p^{i,j,i',j'} |p_{i,j}\rangle\langle p_{i',j'}|$$
$$+ \sum_{i,i'} V_l^{i,i'} |l_i\rangle\langle l_{i'}|, \tag{7}$$

where i (or i') represents a particular atom and j (or j') $= 1, 2$ is a particular bond of this atom. The first, second, and third terms contain interactions among the s orbitals, p hybrid and mixed orbitals, and lone-pair orbitals, respectively. We neglect any other types of interactions. This is not a bad approximation and leaves us with a Hamiltonian that is decoupled and easy to work with. The interactions $V_s^{i,i'}$, $V_p^{i,j,i',j'}$, and $V_l^{i,i'}$ that we have chosen are shown in Fig. 2(b) and have physical interpretations that are easily understood. For $V_S^{i,i'}$ we take

$$V_s^{i,i'} = V_s \delta_{i,i'} + V_s'(1 - \delta_{i,i'}), \tag{8}$$

where V_s represents the position of the center of mass of the s-like band or essentially the atomic s level. V_s' is the interaction between first nearest neighbors and is related to the width of this band. For $V_p^{i,j,i',j'}$ we take

$$V_p^{i,j,i',j'} = V_p \delta_{i,i'} \delta_{j,j'} + V_p' \delta_{i,i'}(1 - \delta_{j,j'}) + V_p'' \delta_{j,j'}(1 - \delta_{i,i'}) + V_p'''(1 - \delta_{j,j'})(1 - \delta_{i,i'}), \tag{9}$$

where V_p represents the center-of-mass energy of the p-like states and lies near the atomic p level. V_p' represents the interaction of different $|p\rangle$ orbitals on the same atom, V_p'' represents the interaction between hybrid orbitals on different atoms but along the same bond ($j = j'$), and V_p''' represents the interaction between hybrid orbitals on different atoms but *not* along the same bond ($j \neq j'$) and in-

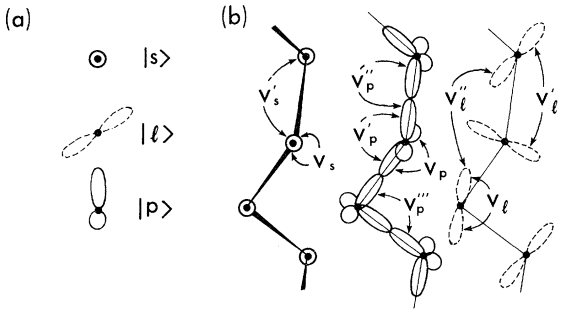

FIG. 2. (a) Schematic representation of the s-like ($|s\rangle$), lone-pair ($|l\rangle$), and mixed and hybridized p-like functions ($|p\rangle$) used in the tight-binding models. (b) Sketch of the respective orbitals along a chain from Fig. 1(a) and the interactions used for the tight-binding model, including only intrachain interactions.

cludes two types of interactions type B and the "dihedral" type D denoted by V_p'''. V_p'' is also responsible for the bonding-antibonding splitting of the p-like states about V_p. Finally, for $V_l^{i,i'}$ we take

$$V_l^{i,i'} = V_l \delta_{i,i'} + I_l^{i,i'}(1 - \delta_{i,i'}), \tag{10}$$

where V_l is the center-of-mass positioned in energy of the lone-pair states and is taken to be different from V_p because of the hybridization of $|p\rangle$. $I_l^{i,i'}$ represents first-nearest-neighbor interactions V_l' and second-nearest-neighbor interactions V_l''. The reasons for including second-nearest neighbors in both $V_l^{i,i'}$ and $V_p^{i,j,i',j'}$ will be discussed later.

The trigonal structure contains only three atoms in a primitive cell; so the eigenvalues and density of states of this Hamiltonian can be obtained analytically quite easily. In particular, the eigenvalues of the hybrid and mixed p-like part of the Hamiltonian can be related by an analytic transformation to the eigenvalues of a much simpler Hamiltonian in which we place only one localized state on an atom and take only nearest-neighbor interactions into account. To show this, consider the chain shown in Fig. 3(a). For any given atom i, we label the coefficients of the $|p\rangle$ orbitals in the total wave function near this atom by a, b, c, etc. For any a_j and b_j (where $j = 1$ or 2) Schrödinger's equation reduces to

$$Ea_j = (a_1 + a_2)V_p' + b_j V_p'' + (c_j + b_k)V_p''', \tag{11}$$

$$Eb_j = (b_j + c_j)V_p' + a_j V_p'' + (a_k + d_j)V_p''', \tag{12}$$

where $j \neq k$ and we have assumed that $V_p = V_p'$ for convenience. If we now sum over k and j we get

$$2E\alpha_i = 4V_p'\alpha_i + 2V_p''\beta_i + 2V_p'''\sum_j \alpha_j, \tag{13}$$

$$2E\beta_i = 2V_p'\sum_j \alpha_j + 2V_p''\alpha_i + 2V_p'''\sum_j \beta_j, \tag{14}$$

where α_i is the sum of the coefficients of $|p\rangle$ associated with atom i and β_i is the sum of the coefficients of $|p\rangle$ associated with the first-nearest-neighbor atoms of atom i which lie along the bond pointing towards atom i. Thus in Fig. 3(a), $\alpha_i = a_1 + a_2$ and $\beta_i = b_1 + b_2$. Equations (13) and (14) can of course be written in terms of a matrix equation of the form

$$\begin{pmatrix} \epsilon & 0 \\ 0 & \epsilon \end{pmatrix} \begin{pmatrix} \hat{\alpha}_i \\ \hat{\beta}_i \end{pmatrix} = \begin{pmatrix} V & 0 \\ 0 & V \end{pmatrix} \begin{pmatrix} \sum_j \hat{\alpha}_j \\ \sum_j \hat{\beta}_j \end{pmatrix}, \tag{15}$$

where $\hat{\alpha}_i$ and $\hat{\beta}_i$ are related by a unitary transformation to α_i and β_i and

$$E = V_p + V_p'''\epsilon/V \pm [(V_p')^2 + (V_p'')^2 + V_p'V_p''\epsilon/V]^{1/2}, \tag{16}$$

where we have taken into account again the difference between V_p and V_p'. Thus the problem of solving the hybrid and mixed p-like part of H in Eq. (7) is reduced to solving the simple system described by

$$\epsilon\hat{\alpha}_i = V\sum_j \hat{\alpha}_j, \tag{17}$$

whose eigenvalues are easily obtained and related to E by Eq. (16). This is similar to the one-band–two-band transformation used by Thorpe and Weaire[14] in the case of tetrahedrally coordinated solids. Using (7), (8), (17), and (16) we obtain for the trigonal case from $0 \leq k \leq \pi/c$ or Γ to A

$$\begin{aligned} E_1^s &= V_s + 2V_s'\cos\tfrac{1}{3}kc, \\ E_2^s &= V_s + 2V_s'\cos\tfrac{1}{3}(kc - 2\pi), \\ E_3^s &= V_s + 2V_s'\cos\tfrac{1}{3}(kc + 2\pi), \end{aligned} \tag{18}$$

$$\begin{aligned} E_1^{pb} &= V_p + 2V_p'''\cos\tfrac{1}{3}(kc + 2\pi) \\ &\quad - [(V_p')^2 + (V_p'')^2 + 2V_p'V_p''\cos\tfrac{1}{3}(kc + 2\pi)]^{1/2}, \\ E_2^{pb} &= V_p + 2V_p'''\cos\tfrac{1}{3}(kc - 2\pi) \\ &\quad - [(V_p')^2 + (V_p'')^2 + 2V_p'V_p''\cos\tfrac{1}{3}(kc - 2\pi)]^{1/2}, \\ E_3^{pb} &= V_p + 2V_p'''\cos\tfrac{1}{3}kc \\ &\quad - [(V_p')^2 + (V_p'')^2 + 2V_p'V_p''\cos\tfrac{1}{3}kc]^{1/2}, \end{aligned} \tag{19}$$

$$\begin{aligned} E_1^l &= V_l + 2V_l'\cos\tfrac{1}{3}kc + 2V_l''\cos\tfrac{2}{3}kc, \\ E_2^l &= V_l + 2V_l'\cos\tfrac{1}{3}(kc - 2\pi) + 2V_l''\cos\tfrac{1}{3}(2kc + 2\pi), \\ E_3^l &= V_l + 2V_l'\cos\tfrac{1}{3}(kc + 2\pi) + 2V_l''\cos\tfrac{1}{3}(2kc - 2\pi), \end{aligned} \tag{20}$$

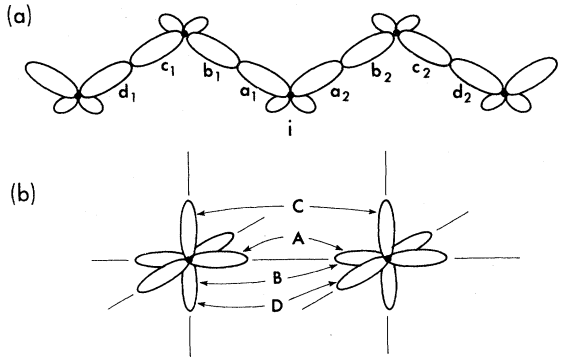

FIG. 3. (a) Sketch of $|p\rangle$ orbitals along a chain with a reference atom i. The letters a_1, a_2, b_1, b_2, etc., represent the coefficients of each $|p\rangle$ orbital in the expansion of the total wave function of the system. (b) Possible nearest-neighbor interactions of p functions in a simple cubic lattice.

$$
\begin{aligned}
E_1^{pa} &= V_p + 2V_p''' \cos\tfrac{1}{3}kc \\
&\quad + [(V_p')^2 + (V_p'')^2 + 2V_p'V_p'' \cos\tfrac{1}{3}kc]^{1/2}, \\
E_2^{pa} &= V_p + 2V_p''' \cos\tfrac{1}{3}(kc - 2\pi) \\
&\quad + [(V_p')^2 + (V_p'')^2 + 2V_p'V_p'' \cos\tfrac{1}{3}(kc - 2\pi)]^{1/2}, \\
E_3^{pa} &= V_p + 2V_p''' \cos\tfrac{1}{3}(kc + 2\pi) \\
&\quad + [(V_p')^2 + (V_p'')^2 + 2V_p'V_p'' \cos\tfrac{1}{3}(kc + 2\pi)]^{1/2},
\end{aligned} \tag{21}
$$

where E^s, E^{pb}, E^l, and E^{pa} represent the s-like, p-like-bonding, lone-pair, and p-like-antibonding bands, respectively. The densities of states for these bands are given by

$$
D_s(E) = \frac{3}{c} \frac{1}{[4(V_s')^2 - (E - V_s)^2]^{1/2}}, \tag{22}
$$

$$
D_p(E) = \frac{3}{c} \frac{1}{(1-\Delta^2)^{1/2}} \frac{2V_p'''\Delta - (E - V_p)}{2EV_p''' - 4(V_p''')^2\Delta - V_p'V_p''}, \tag{23}
$$

$$
D_l(E) = \frac{3}{2c} \frac{1}{(1-\Lambda^2)(V' + 4V''\Lambda)^2}, \tag{24}
$$

where

$$
\begin{aligned}
\Delta &= [2(E - V_p)V_p''' - V_p'V_p'']/4(V_p''')^2 \\
&\quad + \{4(V_p''')^2[(V_p')^2 + (V_p'')^2] - 4(E - V_p)V_p'''V_p''V_p' \\
&\quad + (V_p')^2(V_p'')^2\}^{1/2}/4(V_p''')^2,
\end{aligned} \tag{25}
$$

$$
\Lambda = \{-V_l' + [(V_l')^2 + 8(V_l'')^2 + 4(E - V_l)V_l'']^{1/2}\}/4V_l''. \tag{26}
$$

C. Tight-binding model including interchain interactions

A three-dimensional view of the trigonal structure is shown in Fig. 1(a). As we have already mentioned, the trigonal structure can be changed to a simple cubic structure [Fig. 1(b)] with just a small trigonal distortion. This is very convenient since it provides a very simple way of choosing the most important tight-binding parameters to use in a "three-dimensional" model. The method we will use in selecting a set of tight-binding parameters is the following. We consider the simple cubic structure and obtain all the interactions between nearest-neighbor atoms. We explicitly retain the identity of the individual chains and hence the character of the tight-binding orbitals $|s\rangle$, $|p\rangle$, and $|l\rangle$ as in Sec. III B. In this way each interaction can be classified as an interchain or intrachain interaction. For example, for the $|s\rangle$ orbitals we have six nearest-neighbor interactions, two of which are intrachain (V_s') and four which are interchain (U_s). For the $|p\rangle$ and $|l\rangle$ orbitals (i.e., p-like states) the interactions are a bit more complicated. If we had pure p states in a simple cubic lattice we would only have four nearest-neighbor interactions, as shown in Fig. 3(b). Two of these (types B and D) would have to be zero in this case because of symmetry. For our problem, however, we would need to include all of them. In Fig. 4 we show how the $|p\rangle$ and $|l\rangle$ orbitals would look in a simple cubic structure. Some fragments of the infinite chains are identified by the heavy solid lines. The breakdown of the parameters A, B, C, and D to intrachain and interchain parameters for the various couplings between $|p\rangle$ and $|l\rangle$ orbitals is given in Table I. The usefulness of the simple cubic structure is that we can easily identify all the nearest-neighbor interactions and hence the interactions that remain important under a trigonal distortion. The V and U parameters listed in Table I carry through identically in the trigonal structure and are the p-state parameters we use in our "three-dimensional" tight-binding model. The fitting of these parameters is *not* completely arbitrary and can be performed in a very physical way, as we shall show in detail later when we present the results of our tight-binding models.

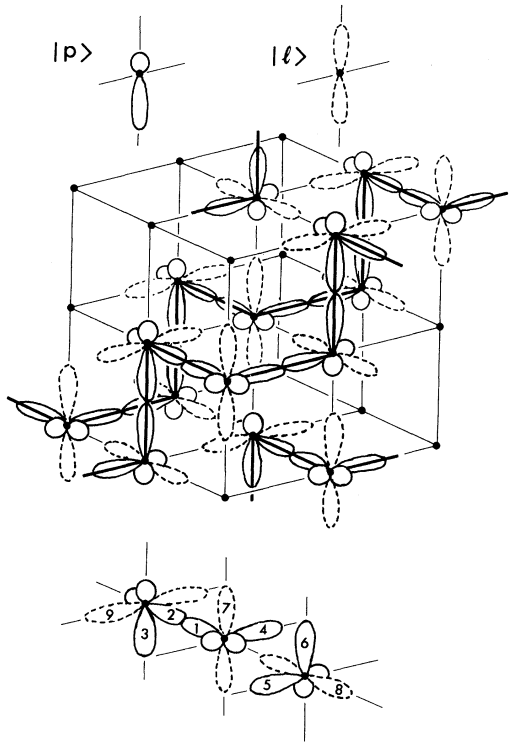

FIG. 4. Arrangement of $|p\rangle$ and $|l\rangle$ orbitals in a simple cubic lattice. The heavy solid lines identify the chains as they would exist in the trigonal structure. A few of the orbitals are labeled to identify the $\langle p|H|p\rangle$, $\langle l|H|p\rangle$, and $\langle l|H|l\rangle$ interactions as used in the tight-binding model, including intra- and interchain couplings. These interaction parameters are listed in Table I.

TABLE I. Interactions between p-like states on different atoms. The first column gives the type of interactions as shown in Fig. 3(b), the second column designates the type of orbitals involved, and the third column gives the total number of interactions per atom. The third and fourth columns give the number of interactions, an example of the specific orbitals involved (see Fig. 4), and the parameter used to designate the interactions for intrachain and interchain coupling, respectively. All intrachain and interchain parameters are labeled V and U, respectively.

Type	Interactions	Total	Intrachain	Interchain
A	$\langle p\|H\|p\rangle$	2	$2(1\|2)V''_p$	
	$\langle l\|H\|p\rangle$	4		$4(1\|8)U_{lp}$
B	$\langle p\|H\|p\rangle$	12	$4(1\|3)V'''_p$	$8(1\|5)U_p$
	$\langle l\|H\|p\rangle$	8	$4(1\|9)V'_{lp}$	$4(4\|8)U'_{lp}$
	$\langle l\|H\|l\rangle$	4		$4(7\|8)U_l$
C	$\langle p\|H\|p\rangle$	4		$4(4\|5)U'_p$
	$\langle l\|H\|p\rangle$	8	$4(4\|9)V''_{lp}$	$4(7\|6)U''_{lp}$
D	$\langle p\|H\|p\rangle$	6	$2(4\|3)V'''_p$	$4(4\|6)U''_p$
	$\langle l\|H\|p\rangle$	4		$4(7\|5)U'''_{lp}$
	$\langle l\|H\|p\rangle$	2	$2(7\|9)V'_l$	

IV. RESULTS FOR TRIGONAL PHASES

A. EPM results

The simple picture of s-like states, bonding and antibonding p-like states and lone-pair states, already confirmed from previous pseudopotential calculations,[5-7,15] is well reproduced by our new pseudopotential calculations, as shown in Fig. 5(a) for Se and 5(b) for Te. The density-of-states spectra were also convoluted with an energy-dependent broadening function (1.2 eV for the s-like states and 0.7 eV for the remaining states) in order to facilitate comparison with experiment. This is shown in Figs. 6(a) and 6(b) together with the experimental UPS and XPS measurements of Shevchik *et al.*[1] for Se and the XPS measurements of Schlüter *et al.*[2] for Te. All observed structures in the experimental spectra are reproduced within 0.3 eV, which is a remarkable improvement over all previous calculations. A very interesting difference between Se and Te appears in the s-like region at energies between −16 and −8 eV. Whereas the density of states for Se s states closely resembles that of a one-dimensional chain (with two singularities at the band-edges), the density of states for the Te s-states looks like a combination of densities of states for a one-dimensional

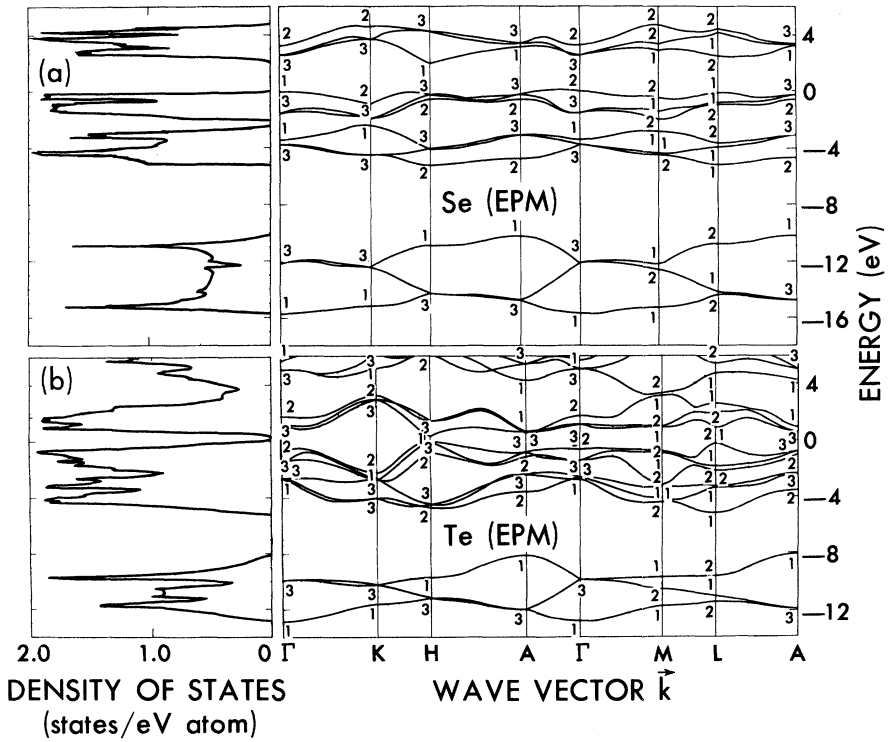

FIG. 5. EPM band structure of trigonal Se (a) and Te (b) along some high-symmetry lines in the hexagonal Brillouin zone. The corresponding densities of states are also given.

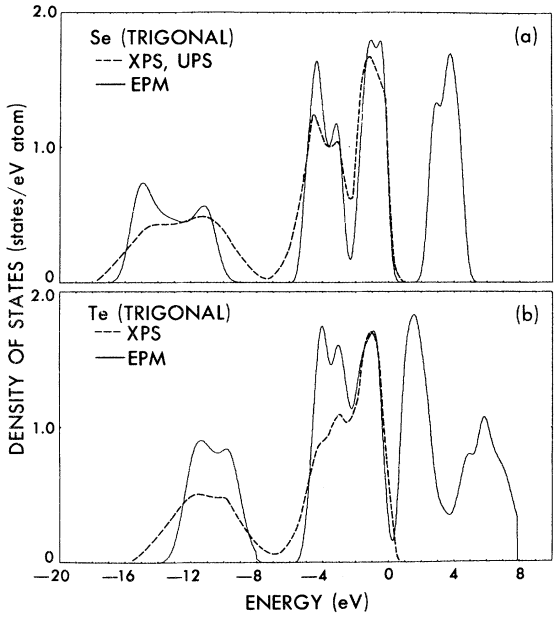

FIG. 6. Calculated densities of states (solid lines) for trigonal Se (a) and Te (b), which for comparison have been broadened by 1.2 eV for the s-like states and by 0.7 eV for the remaining states. Superimposed are the experimental photoemission spectra (dashed lines) for Se and Te as obtained from Refs. 1 and 2, respectively. The scales for the XPS and UPS curves are arbitrary.

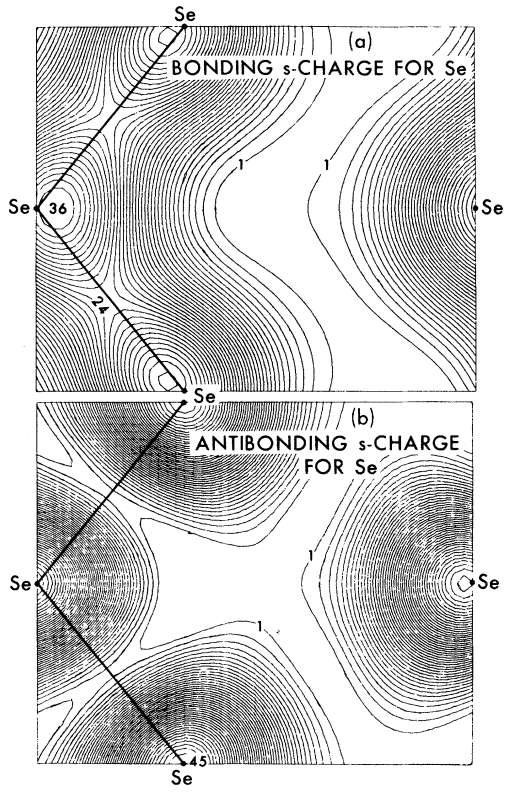

FIG. 7. Calculated charge density for states (a) at the bottom of the s-like band and (b) at the top of the s-like band of trigonal Se. The units are arbitrary and are only to be used for comparison.

chain and a three-dimensional simple cubic lattice. We see here that the s states reflect in a very sensitive way the different degrees of anisotropy found in the two crystals. This sensitivity of the s-states to topology also proves to be a very useful tool in interpreting the amorphous spectra of Se and Te, as we shall see in a later section. It is instructive to display the bonding or antibonding character of the s states close to the two band edges. We therefore show in Figs. 7(a) and 7(b) charge densities for Se obtained from states at the two band edges. The charge distributions are plotted in a plane containing the shaded area of Fig. 1(a). The bonding and antibonding characteristics are clearly displayed. In the bonding states the charge is almost uniformly concentrated along the chains with small excess charges on each atom, whereas in the antibonding states the charge is very strongly concentrated around each individual atom, the wave function having a node between neighboring atoms. One notes that the centers of charge do not exactly coincide with the atomic positions; in fact, they are displaced towards the central axis of the helices for the bonding states and pushed slightly outside the helices for the antibonding states. This asymmetry is compatible with the crystal symmetry, which does not contain spatial inversion. Similar behavior is found for the total charge distribution including all six electrons per atom; here the center of negative charge is displaced towards the center of the helices, thus creating a local static electrical dipole of 0.46 D for Se and 0.60 D for Te on each atom. These approximate values were obtained by integrating over the charge inside touching spheres centered on each atom. The total dipole moment of course vanishes by summing over the unit cell.

The bonding p-like states whose energies vary between −6 and −2.2 eV reveal a very characteristic two-peak structure [see Figs. 6(a) and 6(b)], which is intimately related to two distinct types of bonding states. To understand the origin of the characteristic two-peak structure we have calculated the electronic charge distributions of states in each peak. This entails summing in Eq. (2) over states whose energies (in eV) fall within [−6.0, −3.6] and [−3.6, −2.25] for Se and [−6.0, −3.5] and [−3.5, −2.2] for Te. The resulting charge-density contour plots are shown in Figs. 8(a)–8(d). We find the result that the lower energy peak in the p-like bonding states corresponds to states

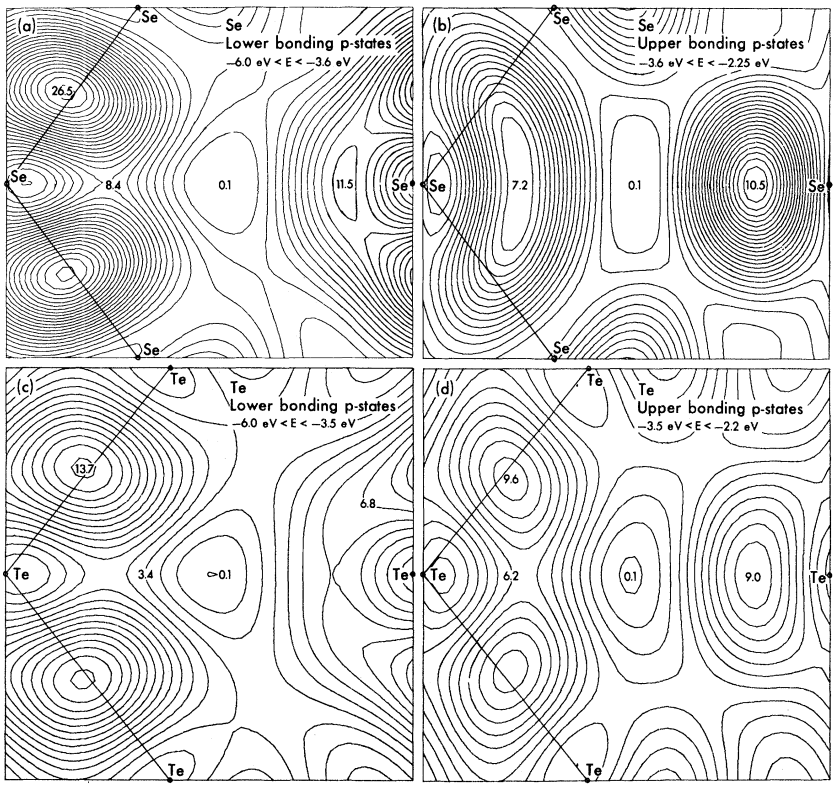

FIG. 8. Calculated charge densities for Se, (a) and (b), and Te, (c) and (d), for the lower, (a) and (c), and upper, (b) and (d), p-like bonding states. The energy intervals are indicated. The values are in units of e/Ω.

which are almost exclusively involved in intrachain bonding. The charge is well localized in the bonds between neighboring atoms belonging to the same chain. There is no important charge accumulation found between the chains. The upper or higher energy peak contains states which in part arise from a mixing of p_x and p_y functions due to a bond angle $\neq 90°$. However, the charge concentrations in the right-hand parts of Figs. 8(b) and 8(d) are, as we shall see, direct consequences of interchain bonding and might thus be viewed as bonding charges. The pure intrachain bonding states lie lower in energy than the states contributing to interchain bonding since the potential is strongest between neighboring atoms within a chain. A direct proof of the importance of covalent interchain bonding in Se and to a lesser extent in Te was obtained in the following way: We repeated the complete calculations for Se with identical potential parameters and identical intrachain spacings but with an interchain distance increased by about 20%. This increase of interchain distance should considerably decrease all interchain bonding charges and thus exhibit their importance in the normal trigonal phase. We first discuss some changes in the density of states calculated for this new structure, which we shall call Se2. In the s-like region only very small changes towards a more one-dimensional behavior can be recognized. The width of the characteristic two-peak splitting of the bonding p-like states remained unaltered. As we shall see in the discussion of possible amorphous phases, this width is sensitive to the bond angles within the chains. The relative weight of the two peaks in Se2 changed somewhat with respect to Se. The lower-energy peak increased, whereas the upper or higher-energy peak decreased, thus already indicating a decrease in the interchain bonding strength. An equivalent behavior was of course observed for the unoccupied antibonding p-like states. The lone-pair peak remained essentially unaltered with respect to its shape and its position. A very clear picture of the importance of interchain bonding in Se can be obtained by comparing the corresponding charge distributions of Se and Se2. In an attempt to focus intention on bonding charges we extracted the short-wavelength Fourier components of the charge-density functions and thus separated out the slowly varying background charge, as discussed in Sec. III A. This separation was simply achieved by considering the charge-density Fourier series starting at a cutoff wavelength λ_0. For the extraction of bond charges this cutoff was found to lie natu-

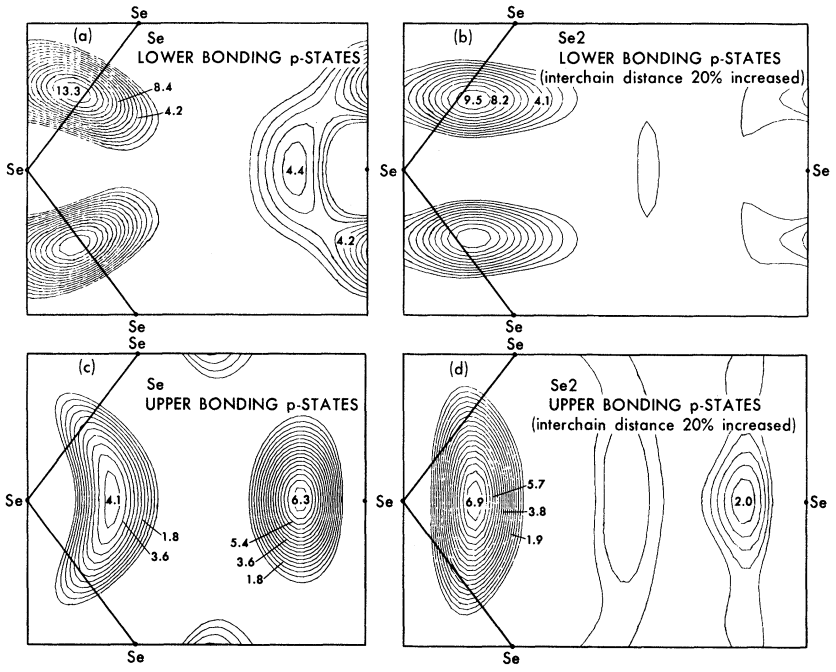

FIG. 9. Bonding charges of trigonal Se, (a) and (c), and of a model structure of Se, (b) and (d), in which the interchain distance has been increased by 20%. The charges have been calculated for the lower, (a) and (b), and upper (c) and (d), p-like bonding states, retaining only short-wavelength components, as described in the text. Only positive contours are shown, with values in units of e/Ω.

rally at $\lambda_0 = d$, where d is the nearest-neighbor distance within the chains of Se. No spurious oscillations in the density distribution occur, if only the positive contributions of the restricted Fourier series to the total charge are considered. The results obtained for Se and Se2 by retaining only Fourier components with $\lambda \leq \lambda_0$ are shown in Figs. 9(a)–9(d). By comparing Figs. 9(a) and 9(c) with the corresponding total charge densities of Se [see Figs. 8(a) and 8(b)] one can verify the effect of extracting the short-wavelength Fourier components in the charge distribution. The most interesting differences between the charge densities of Se and Se2 are found in the higher-energy region of the p-like bonding states. The charge pile up in Se in the right-hand part of Fig. 9(c) disappears almost completely in Se2 [Fig. 9(d)]. This confirms our previous interpretation of this charge's contributing to the interchain bonding. The decrease of interchain bonding in Se2 is coupled to an increase of intrachain bonding as seen from the rearrangement of charge in Se2 and from the changes in the density of states. We are now in a position to define some measure of intrachain vs interchain bonding strength in Se and Te by calculating the magnitude of the respective bonding charges. By integrating the charge in Figs. 9(a) and 9(c) we find for Se $0.07e^-$ for the intrachain bond and $0.04e^-$ for the interchain bond. It is instructive to compare these values with $0.05e^-$ and $0.04e^-$ for the intra- and interchain bonding charges of Te. The ratio ξ of intrachain to interchain bonding charge decreases from 1.75 for Se to 1.25 for Te and thus reflects the more three-dimensional or more isotropic character of Te. The smaller amount of total bonding charge in Te is indicative of its more metallic or less covalent character. The absolute values of the charges of course depend strongly on the definition of bonding charges. The indicated values should therefore by considered as a relative measure rather than individually.

B. Tight-binding results

The tight-binding models we introduced in Sec. III provide a means of understanding, in a very simple way, the band structures obtained using the more realistic EPM. Certain general features in these band structures (Fig. 5) can be interpreted physically in terms of the type, sign, and magnitude of the real space interactions involved.

We begin with the simple tight-binding model with only intrachain parameters. The energy bands (18)–(21) and the associated densities of states (22)–(26) are plotted in Fig. 10. Here we have taken $V_s = -13.0$, $V_s' = -1.3$, $V_p = -0.2$, $V_p' = 0$, $V_p'' = 3.8$, $V_p''' = 0.55$, $V_t = -1.3$, $V_t' = 0.4$, and $V_t'' = 0.26$. These parameters are given in units of eV and are shown schematically in Fig. 2. They were fitted to the EPM band structure of Se plotted in Fig. 5. We note that the over-all agreement with the Se EPM band structure and density of states is quite satisfying considering the approximations we are making here. In particular, the band structure and density of states of the s-like

states of the tight-binding model compare surprisingly well with those of Se in Fig. 5.

The prominent features of the p-like states for Se in Fig. 5 are also reproduced to some extent in Fig. 10. The parameter V_p'' represents interactions between orbitals along the same bond and is responsible for the formation of bonding and antibonding bands. To broaden the bands we could introduce an interaction V_p' between different orbitals on the same atom. However, this would put A_3 and Γ_2 lower in energy than A_1 and Γ_3, respectively, in the antibonding bands. To obtain the correct ordering, we must include an interaction V_p''' between orbitals on nearest-neighbor atoms which are *not* along the same bond. In addition, V_p' must be small. This is consistent with the fact that the $|p\rangle$ orbitals are very p-like in nature with a rather small hybridization of s and d. For simplicity we take V_p' equal to zero.

The shape of the lone-pair bands of Se in the EPM calculation is also reproduced rather well in Fig. 10. To get the correct band ordering at Γ and A it is necessary to include both first-nearest-neighbor V_l' and second-nearest-neighbor V_l'' interactions between $|l\rangle$ orbitals. In particular, V_l' and V_l'' need to be positive with $V_l' > V_l''$.

To improve the tight-binding Se results and to interpret the EPM Te results it is necessary to introduce interchain parameters. This is quite clear from the s-like region of the density of states of Te (Fig. 5), where a "three-dimensional" simple-cubic-like density of states structure appears in the middle of the band. The band structures and densities of states of Se and Te using the tight-binding model including interchain interactions (discussed in Sec. III C) are shown in Fig. 11. The symmetries of the energy levels are assumed to be the same as those for the EPM calculations. We notice that the general agreement between the densities of states and band structures in Fig. 5 and Fig. 11 is rather good. The parameters used in these tight-binding calculations are listed in Table II. These parameters are not meant to represent the best fits using this model but rather to give a flavor of the type of interactions involved in reproducing the general features of the more realistic EPM band structures. Although the $|p\rangle$ and $|l\rangle$ interactions seem to be many, they are not physically completely independent and were not adjusted arbitrarily. As we have already mentioned, the trigonal structure of Se and particularly Te is rather close to that of a

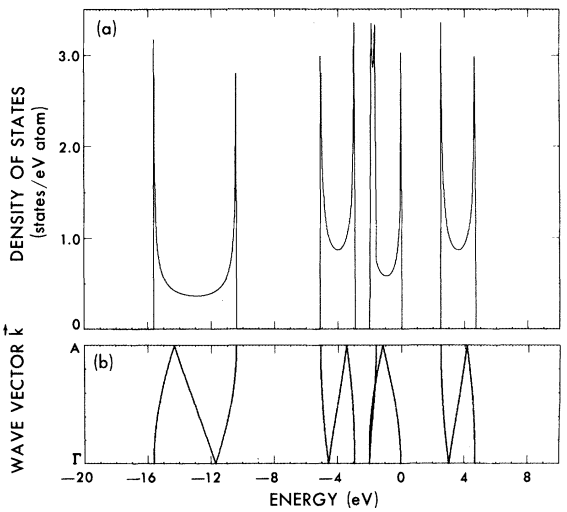

FIG. 10. Density of states (a) and band structure (b) obtained using the tight-binding model, including only intrachain interactions. The parameters of this "one-dimensional" tight-binding model are discussed in the text.

TABLE II. Interactions and parameters used in the tight-binding model including intrachain (V) and interchain (U) interactions for Se and Te. The parameters are defined in the text and are given in units of eV.

Type	Se	Te
V_s	−13.1	−10.6
V_s'	−1.1	−0.7
U_s	−0.1	−0.25
V_p	−0.2	−1.0
V_p'	0	0
V_p''	3.4	2.2
U_{lp}	0.7	1.0
V_p'''	0.4	0.2
U_p	0.2	0.15
V_{lp}'	0.2	0.2
U_{lp}'	0.1	−0.1
U_p'	−0.05	−0.2
V_{lp}''	−0.7	−0.7
U_{lp}''	−0.3	−0.4
V_p''''	0	−0.1
U_p''	−0.3	−0.25
U_{lp}'''	−0.1	0.1
V_l	−1.0	−1.2
V_l'	0.2	0.2
V_l''	0.1	0.1
U_l	0	0

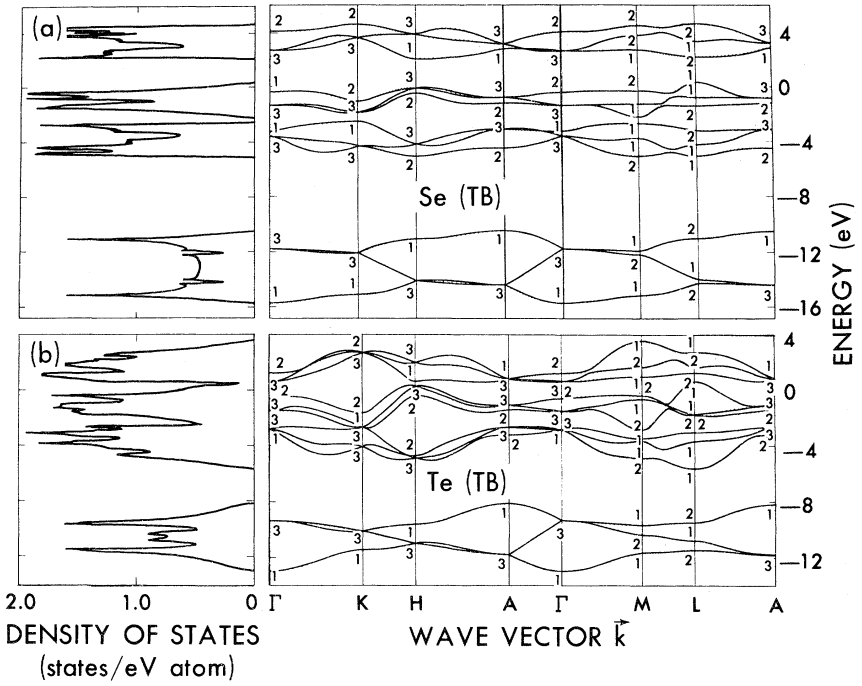

FIG. 11. Densities of states and corresponding band structures for Se (a) and Te (b) as obtained from the tight-binding (TB) model, including intra- and interchain parameters. The parameters of this "three-dimensional" model are discussed in the text, with their values listed in Table II.

simple cubic structure (Fig. 1). We start therefore with an EPM calculation of simple cubic Te. In the tight-binding model we now only have interactions A, B, C, and D [Fig. 3(b)] for the p-like functions and $V_s' = U_s$ (Sec. III C) for the s-like functions. Interactions B and D however are now zero because of symmetry. Let us investigate the p-like states first. If we plot the EPM simple cubic band structure along the same symmetry points and lines as in Figs. 5 and 11 we would find at Γ and K a sixfold degenerate and a three-fold degenerate p-like energy level. These levels of course represent the "bonding and lone-pair" states and the "antibonding" states, respectively, in the trigonal structure. The correct ordering of these levels in the tight-binding model demands that A be positive. By fitting the various parameters to the EPM simple-cubic band structure we get values around $V_p'' = U_{1p} \sim +2$ eV and $U_p' = V_{1p}'' = U_{1p}'' \sim -0.5$ eV.

Let us now break the simple cubic symmetry by introducing a trigonal distortion or equivalently (in the tight-binding model) by taking the difference between intrachain (V) and interchain (U) interactions explicitly into account. Physically we would expect the V parameters in general to be larger in magnitude than the U parameters. Since the cubic symmetry is broken interactions B and D are no longer zero. This has some very important consequences for the band structure. We first consider interactions B. To obtain the correct ordering of the doublet and singlet levels at K, H, A, and Γ as shown in Figs. 5 and 11 it is necessary (as in the one-dimensional model) to take V_p''' positive.

Let us now examine interactions of type D (Table I). Here U_p'' is the only parameter that can change the relative size of the Γ_1-Γ_3 and K_1-K_3 gaps of the bonding states and the H_3-H_1 and A_3-A_1 gaps of the antibonding states.

For the s-like states everything is much simpler. Fitting V_s' and U_s to the simple cubic band structure we get $V_s' = U_s \sim -0.5$. By taking $|V_s'| > |U_s|$ we get all the correct dispersions and band orderings. We should emphasize again that the s-like states are a very useful and convenient system to study because of their sensitivity to topology and their simplicity. The differences in anisotropy of Se and Te are clearly and unambiguously demonstrated by just comparing the values V_s' and U_s for Se with those of V_s' and U_s for Te. As seen from Table II, Se is definitely more anisotropic. This is also revealed in general by comparing the appropriate V and U parameters of Se with those of Te for the p-like functions as shown in Table II.

V. RESULTS FOR AMORPHOUS PHASES

The electronic properties of the amorphous phases of Se and Te have been studied in several papers.[7] The results of theoretical models have usually been compared to experimental optical measurements. Such comparisons are relatively difficult and no conclusive results in particular

concerning the structural nature of the amorphous phases could be obtained. With the advent of new XPS and UPS measurements[1,2] important direct information about *all* the valence bands became available. Moreover, since these measurements were carried out on both crystalline and amorphous phases, a comparative study becomes possible.

Let us now examine the characteristic changes between the crystalline and amorphous phases. We thus show in Fig. 12 (top) the photoemission results of Shevchik *et al.*[1] for trigonal and amorphous Se. The samples were prepared by dc sputtering in a argon atmosphere. The trigonal crystalline phase was obtained by subsequent annealing. The overall structure of the trigonal and amorphous spectra remains essentially unaltered. In particular, *no* broadening with respect to the crystalline phase can be observed in the amorphous phase. This experimental fact is in disagreement with the theoretical model developed by Kramer and co-workers,[7] which is based on short-range order and a specific form of long-range disorder and which gives rise to broadening effects.

In the lone-pair region (between −2 and 0 eV) the amorphous spectrum has lost some fine-structure and perhaps is shifted slightly to higher energies. We may conclude from this that the nonbonding p states remain essentially unaltered in the amorphous phase and do not hybridize noticeably. However, in the bonding p-like region (between −6 and −2 eV) very interesting changes have occurred. The lower-energy peak has become weaker whereas the higher-energy peak increased in the amorphous phase. On the basis of our analysis of the crystalline case we suggest that this reversal corresponds to a decrease of the number of pure intrachain bonding states. As a consequence there are now more electrons occupying states which are partially localized *outside* the chains. By performing several model calculations of trigonal phases of Se with various bond angles (the nearest intra- and interchain distances were kept constant) we found that the splitting in the bonding p-like states is very sensitive to bond angle variations and hence to the mixing. In particular we found that for chains with 90° bond angles the splitting disappeared because of the equivalence of the two different p states. For bond angles $\gtrsim 120°$ the splitting also decreased because of an increase in interaction with the lone-pair states. In the amorphous phase, however, this splitting remains essentially unchanged, thus suggesting that bond-angle variations are relatively small.

A very unusual effect appears in the s-like region (between −18 and −7 eV) of Se. The dip in the photoemission curve seems to be deeper in the amorphous phase than in the crystalline phase. Since we know that the density of s-like states is very sensitive to topology, this effect indicates some very interesting structural properties. For example, it could not be caused by just a breaking of the infinite chains, since this would rather tend to fill up the dip in the density of states, unless the broken chains were of order two, which seems rather unlikely because of the preference of Se for two-fold coordination. A reasonable explanation of the increase of the dip, however, is the formation of some type of rings. In particular, the dip would increase if the rings were of order three, five, six, or seven. Rings of order four, eight, or five and seven together would certainly tend to fill up the dip in the density of states.[16] Furthermore, since the bond angles in the trigonal phase are about 104° and since bond-angle variations seem to be small, the most likely ring structures would be of type fivefold and sixfold, or sixfold and sevenfold. To demonstrate the effect of the existence of rings on the density of states, we have carried out two different model calculations on Se containing only sixfold and only eightfold rings. The rings were arranged in layerlike configurations so that bond angles, nearest-neighbor distances, and second-nearest-neighbor distances were identical to those in the trigonal form. The resulting densities of states are shown in Fig. 13. We notice that the structure in the s-like region

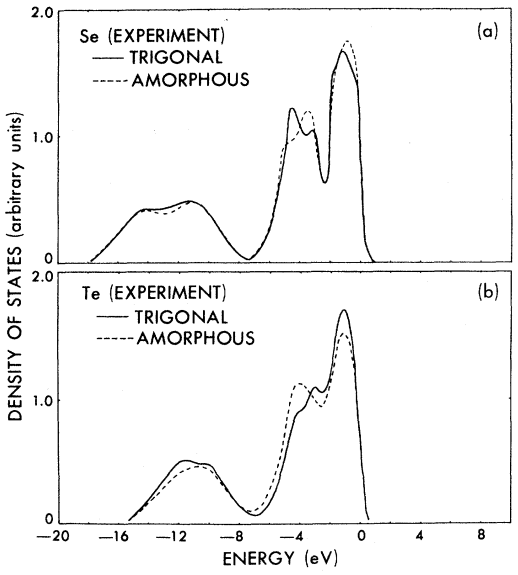

FIG. 12. X-ray and ultraviolet photoemission results (top) on trigonal (solid line) and amorphous (dashed line) Se as obtained from Ref. 1. X-ray photoemission results (bottom) on trigonal (solid line) and amorphous (dashed line) Te as obtained from Ref. 2.

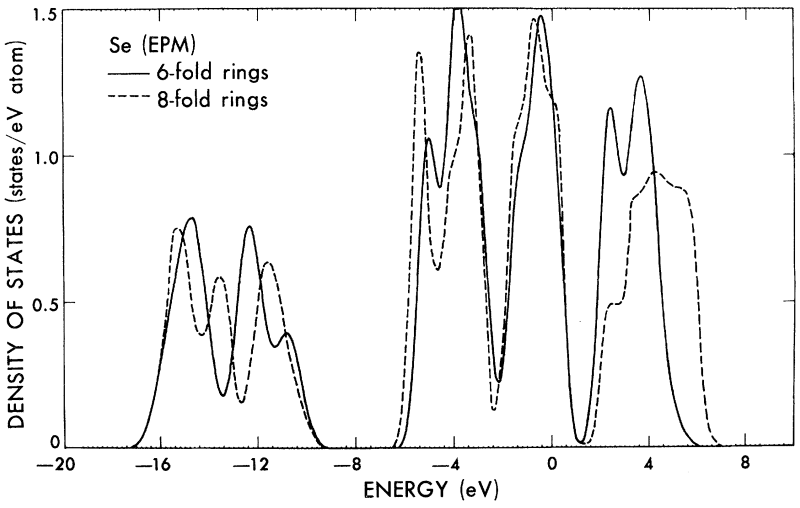

FIG. 13. Density of states of Se in model structures containing only six-fold (solid line) and only eight-fold (dashed line) rings of atoms as obtained from EPM calculations. The curves are broadened as in Fig. 6.

behaves essentially as expected for isolated rings. The sixfold ring configuration gives rise to a pronounced dip in the middle of the density of states, while the eightfold ring structure adds a peak in this region. In the p-like bonding region we essentially obtain the same results as in the experimental amorphous spectrum, i.e., a shift of strength to higher energies. It is not clear, however, whether this shift is a consequence of ring resonances or of the different inter-ring environment.

On the basis of this analysis we propose that the amorphous Se sample used in the photoemission measurements of Shevchik *et al.*[1] contains a substantial number of atoms in ring-like configurations of order six, five, and maybe seven. This suggestion seems to be consistent with Rechtin and Avenbachs[17] interpretation of their radial-distribution-function data. The existence of a substantial number of eightfold rings, as often proposed for amorphous Se,[1] seems to be a rather questionable possible structural feature for this sample.

The photoemission results for crystalline and amorphous Te obtained by Shevchik *et al.*[1] using the same sputtering technique as for their Te sample give similar results. However, these results differ considerably from photoemission data on amorphous Te prepared by argon bombardment.[2] The latter results are shown in Fig. 12 (bottom) together with the crystalline spectrum obtained on the same sample before argon bombardment. As in Se the lone-pair regions remain relatively unaltered. In the bonding p-like region (between −6 and −2 eV) we find in contrast to Se a shift of strength to *lower* energies. This suggests an *increase* in the number of pure intrachain bonding states, which is consistent with an increase of covalency of Te in the amorphous phase. The structural information derived from the density of states in the s-like region is somewhat more difficult to discern since there now seems to be a filling up of the dip in the amorphous case. In spite of the fact that the structure of trigonal Te is close to the simple cubic structure, regions of simple cubic structure can be dismissed, since these would give rise to a merging of the p-like bonding states with the lone-pair states. What remains therefore is to discern between structures which contain mostly broken chains or broken chains with a substantial amount of rings. It is, however, rather difficult to make a conclusive statement about the structure of this sample of amorphous Te without better experimental resolution. One could speculate that argon bombardment tends to leave the system with atoms existing mostly in broken-chain configurations. On the other hand, sputtering and the deposition of thin films may favor the formation of rings.

VI. SUMMARY AND CONCLUSIONS

We have presented a detailed study of the density of states of trigonal Se and Te. This was accomplished by first performing new EPM calculations which give an excellent fit to recent photoemission measurements.[1-3] This enabled us to perform charge density calculations associated with specific peaks in the density of states. In particular, the characteristic two-peak structure in the bonding p-like states is interpreted as involving intrachain bonding (lower-energy peak) and interchain bonding (higher-energy peak) states. This interpretation is confirmed by pulling the chains apart and finding that the localized charge between the chains is greatly reduced while the lone-pairs,

etc. remain relatively unchanged. Thus this type of "bonding" must be added to the van der Waals interaction to obtain the total interaction between the chains. In addition, we have calculated the amount of s and d character in the p-like region. We find in general a presence of around (5–10)% s and (1–5)% d character in the wave functions. This p-d admixture should be enough to change the bond angle from 90° to 104° without involving a strong s-p admixture. A strong s-p admixture as suggested by Chen[4] to account for the 104° bond angle is not necessary and not supported by the recent photoemission results.[1-8]

We have also introduced a "one-dimensional" and "three-dimensional" tight-binding model which includes only intrachain and intra- and interchain interactions, respectively. The results show the closely "one-dimensional" or strongly anisotropic nature of Se and the sensitivity of the s-like states to topology. The "three-dimensional" tight-binding model is introduced to get a better description of Se and to treat the relatively more isotropic Te. By fitting the band structures of this model to those of Se and Te using the EPM it is easy to identify the most important real space orbital-orbital interactions and therefore obtain a physical understanding of the origins of various features in the band structures.

With a good understanding of the trigonal forms of Se and Te at hand, we have analyzed the changes observed in the photoemission spectra of amorphous Se and Te. In particular there are changes between the trigonal spectra and the amorphous spectra, and differences between the amorphous spectra depending on sample preparation.

---

†Supported in part by the National Science Foundation Grant No. GH 35688.

*Present address: Department of Physics, MIT, Cambridge, Mass.

‡Swiss National Science Foundation Postdoctoral Fellow.

[1]N. J. Shevchik, J. Tejeda, M. Cardona, and D. W. Langer, Solid State Commun. 12, 1285 (1973); N. J. Shevchik, M. Cardona, and J. Tejeda, Phys. Rev. B 8, 2833 (1973).

[2]M. Schlüter, J. D. Joannopoulos, M. L. Cohen, L. Ley, S. Kowalczyk, R. Pollak, and D. A. Shirley, Solid State Commun. 15, 1007 (1974); M. Schlüter, J. D. Joannopoulos, and Marvin L. Cohen, Phys. Rev. Lett. 33, 89 (1974); 33, 337 (1974); T. Ichikawa, J. Phys. Soc. Jpn. 36, 1213 (1974).

[3]R. A. Powell, W. E. Spicer, Phys. Rev. B 10, 1603 (1974).

[4]S. Tutihasi and I. Chen, Phys. Rev. 158, 623 (1967); I. Chen, Phys. Rev. B 7, 3672 (1973).

[5]R. Sandrock, Phys. Rev. 169, 642 (1968).

[6]K. Maschke, Phys. Status Solidi B 47, 511 (1971).

[7]B. Kramer, K. Maschke, and L. D. Laude, Phys. Rev. B 8, 578 (1973), and references therein.

[8]M. L. Cohen and V. Heine, in *Solid State Physics*, edited by H. Ehrenreich, F. Seitz, and D. Turnbull (Academic, New York, 1970), Vol. 24, p. 37.

[9]F. Hulliger and E. Mooser, in *Progress in Solid State Chemistry* (Pergamon, Oxford, 1965), Vol. 2, p. 330.

[10]J. Stuke, in *The Physics of Se and Te*, edited by W. C. Cooper (Pergamon, Oxford, 1969), p. 3.

[11]P. Löwdin, J. Chem. Phys. 19, 1396 (1951).

[12]G. Gilat and L. J. Raubenheimer, Phys. Rev. 144, 390 (1966).

[13]J. P. Walter and Marvin L. Cohen, Phys. Rev. B 4, 1877 (1971).

[14]M. F. Thorpe and D. Weaire, Phys. Rev. B 4, 3518 (1971).

[15]M. Schlüter, Int. J. Quantum Chem. 7, 527 (1973).

[16]J. D. Joannopoulos, F. Yndurain, L. Falicov, and M. L. Cohen, AIP Conf. Proc. 20, 167 (1974).

[17]M. D. Rechtin and B. L. Averbach, Solid State Commun. 13, 491 (1973).